ACS OMEGA

Open Access

http://pubs.acs.org/journal/acsodf

Article

Proteoglycan Extracted from *Ganoderma lucidum* Ameliorated Diabetes-Induced Muscle Atrophy via the AMPK/SIRT1 Pathway In Vivo and In Vitro

Published as part of the ACS Omega virtual special issue "Phytochemistry".

Jiaqi Li, Ying Zhang, Fanzhen Yu, Yanna Pan, Zeng Zhang, Yanming He,* Hongjie Yang,* and Ping Zhou*

Cite This: *ACS Omega* 2023, 8, 30359−30373

Read Online

ACCESS | Metrics & More | Article Recommendations | Supporting Information

ABSTRACT: Muscle atrophy often occurs in type 2 diabetes (T2D) and leads to an increase in physical disability and insulin resistance. However, there are very few studies that have investigated potential natural products used for this condition. In this study, we demonstrated that *FYGL* (Fudan-Yueyang-*G. lucidum*), a proteoglycan extracted from *Ganoderma lucidum*, ameliorated muscle atrophy in rat and mouse models of diabetes. Histopathological analysis of muscle revealed that oral administration of *FYGL* significantly prevented reduction of the cross-sectional area of muscle fibers and overexpression of muscle atrophic factors in diabetic rats and mice. Muscle RNA-seq analysis in vivo indicated that *FYGL* regulated genes related to myogenesis, muscle atrophy, and oxidative phosphorylation. Also, *FYGL* activated AMPK in vivo. Furthermore, the underlying molecular mechanisms were studied in palmitate-induced C2C12 muscle cells using immunofluorescence staining and Western blotting, which revealed that *FYGL* inhibited muscle atrophy by stimulating ATP production and activating the AMPK/SIRT1 pathway, thus promoting oxidative metabolism. This result rationalized the in vivo findings. These results suggest *FYGL* as a promising functional food ingredient for the prevention of T2D-induced muscle atrophy.

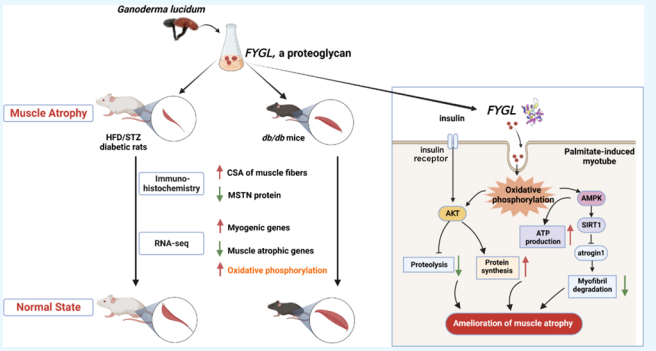

1. INTRODUCTION

Muscle atrophy often occurs in patients with diabetes mellitus and is characterized by a loss of muscle mass and a decrease in muscle strength, leading to physical disability.[1,2] Reduced muscle mass results in impaired glucose and lipid homeostasis and promotes the progression of type 2 diabetes (T2D).[3] The degradation of protein and a decrease in protein synthesis in the skeletal muscle accelerate muscle mass loss. During the process of muscle atrophy, *MURF1* (muscle RING-finger 1) and *atrogin 1* are significantly up-regulated and play an important role in the degradation of muscle proteins. Thus, these two genes are regarded as markers of muscle atrophy.[4,5]

Research has shown that mitochondrial dysfunction plays an important role in mediating muscle atrophy in T2D. Promoting mitochondrial biogenesis and oxidative metabolism is beneficial in the treatment of T2D-induced muscle atrophy.[6−8] In addition, AMP-activated kinase (AMPK) is crucial to the fundamental regulation of energy balance and oxidative metabolism.[9] It has been reported that AMPK agonists have the potential to prevent muscle atrophy in streptozotocin-induced diabetic rats.[10] Additionally, activation of AMPK stimulates the activity of sirtuin 1 (SIRT1), also an important regulator of mitochondrial biogenesis.[11] Shen et al. reported that activation of SIRT1 suppressed the overexpression of *atrogin 1* in the skeletal muscle, preventing dexamethasone-induced muscle atrophy.[12] Therefore, activating the AMPK/SIRT1 pathway and promoting oxidative metabolism are considered a potential therapeutic approach in the treatment of T2D-induced muscle atrophy. However, few therapeutic drugs for muscle atrophy, such as recombinant growth hormone and megestrol acetate, are available in clinical practice. The side effects resulting from these drug treatments include insulin resistance, peripheral edema, and transient adrenal insufficiency. Unlike chemical drugs, natural products

Received: May 19, 2023
Accepted: July 27, 2023
Published: August 8, 2023

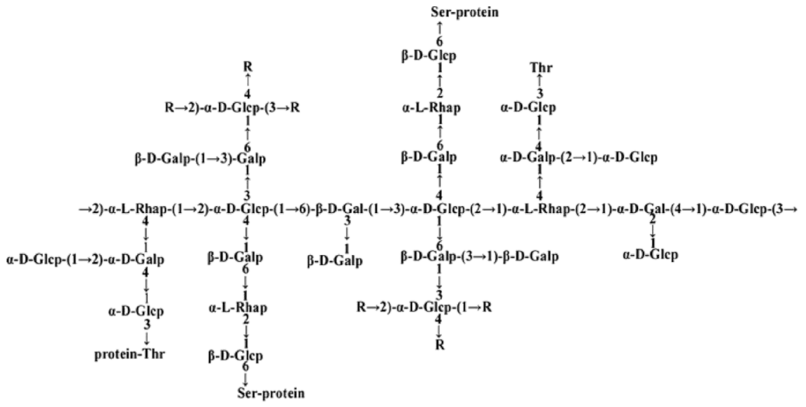

(A)

MEDEVAALVI DNGSGMCKAG FAGDDAPRAV FPSIVGRPRH QGVMVGMGQK DSYVGDEAQS$_{60}$
KRGVLTLKYP IEHGIVTNWD DMEKIWHHTF YNELRVAPEE HPVLLTEAPL NPKANREKMT$_{120}$
QIMFETFNAP AFYVAIQAVL SLYASGRTTG IVLDSGDGVT HTVPIYEGFS LPHAILRIDL$_{180}$
AGRDLTEFLI KNLMERGYPF HTTAEREIVR DIKEKLCYVA LDFEQELQTA AHSSALEKSY$_{240}$
ELPDGQVITI GNERFRAPEA LFQPAFLGLE AAGIHETTYN SIYKCDLDIR RDLYGNIVLS$_{300}$
GGTTMFPGIA DRMQKELTAL APSSMKVKIV APPERKYSVW IGGSILASLS TFQNLWCSKQ$_{360}$
EYDESGPGIV HRKCF$_{375}$

(B)

Figure 1. (A) Dominant structure of *FYGL*. Gal: galactose, Glc: glucose, Rha: rhamnose, Ara: arabinose. Thr: threonine, and Ser: serine. The polysaccharide moieties of *FYGL* covalently bind to the serine and threonine residues of protein moieties via O-type glycoside.[17] (B) Dominant sequence of the protein moieties of *FYGL*.[24]

have the unique advantage of causing few side effects. Therefore, there is an unmet medical need to explore functional components from natural resources for protection against diabetes-induced muscle atrophy.

Ganoderma lucidum is widely known for its antiaging and anti-inflammatory activities and has been used medicinally for more than 2000 years.[13−15] Previously, we extracted a proteoglycan with a molecular weight of 2.6×10^5 Da from *Ganoderma lucidum*, which we named *FYGL* (Fudan-Yueyang-*G. lucidum*).[16] Chemical and spectroscopic methods were used to characterize the dominant structure of *FYGL* (Figures S1−S6).[17,18] As shown in Figure 1A,B, the polysaccharide moieties of *FYGL* consist of arabinose, galactose, rhamnose, and glucose. These moieties covalently bind to the serine and threonine residues of protein moieties in *FYGL via* O-type glycoside. It was previously demonstrated that *FYGL* ameliorated skeletal muscle insulin resistance in vivo by suppressing the expression of protein tyrosine phosphatase 1B (PTP1B).[19] However, the effects and underlying mechanisms of *FYGL* on muscle atrophy in T2D remain unclear.

Palmitate is a saturated fatty acid. It has been reported that exposure of muscle cells to palmitate leads to the accumulation of specific lipid metabolites and subsequent impaired insulin signaling.[20,21] Further, palmitate significantly reduced myotube diameter and up-regulated the expression of atrophic genes such as *atrogin 1* in C2C12 cells.[22,23] Therefore, palmitate-induced C2C12 cells are used as model cells to study the effects of agents on muscle atrophy in T2D in vitro.

In the current study, the role of *FYGL* in preventing diabetes-induced muscle atrophy is evaluated in two diabetic rodent models in vivo, and the underlying mechanisms are further elucidated in palmitate-induced C2C12 cells in vitro.

2. RESULTS

2.1. *FYGL* Ameliorated Muscle Atrophy in Diet-Induced T2D Rats. The effects of *FYGL* on muscle atrophy in diet-induced T2D were investigated in 4-week old male Sprague Dawley (SD) rats that were fed a normal diet (NC rats) or a high-fat diet plus streptozotocin (HFD/STZ rats). After the diet-induced T2D model was established, HFD/STZ rats were orally administrated *FYGL* or saline for 4 weeks. Basic metabolic data of SD rats have been studied and published previously,[25] as shown in Figure S7. In this study, the tibialis anterior (TA) muscle of the rats was dissected, and the inhibitory effects of *FYGL* on muscle atrophy were observed by hematoxylin & eosin (H&E) staining. The cross-sectional area (CSA) of muscle fibers in the HFD/STZ group was reduced by 32% ($P < 0.001$) compared to the NC group. However, *FYGL* or metformin (Met) treatment prevented HFD/STZ-induced reduction of CSA of muscle fibers (Figure 2A,B).

Then, the expressions of protein involved in muscle atrophy were detected to further evaluate the inhibitory effects of *FYGL* on muscle atrophy in HFD/STZ rats. Myostatin (MSTN) is a negative regulator of muscle growth.[26] MSTN negatively regulates muscle mass through the activation of *MURF1* and *atrogin 1*, two muscle-specific ubiquitin ligases regarded as markers of muscle atrophy.[27,28] TA muscle sections were immunohistochemically stained for MSTN expression. MSTN expression was significantly increased in the HFD/STZ group compared with the NC group. This increase was inhibited by *FYGL* or Met treatment (Figure 2C,D). *Atrogin 1* is a muscle-specific ubiquitin ligase that accelerates protein degradation, particularly the degradation of myofibrillar components in the skeletal muscle.[4] Therefore, it is widely used as a marker of

https://doi.org/10.1021/acsomega.3c03513
ACS Omega 2023, 8, 30359−30373

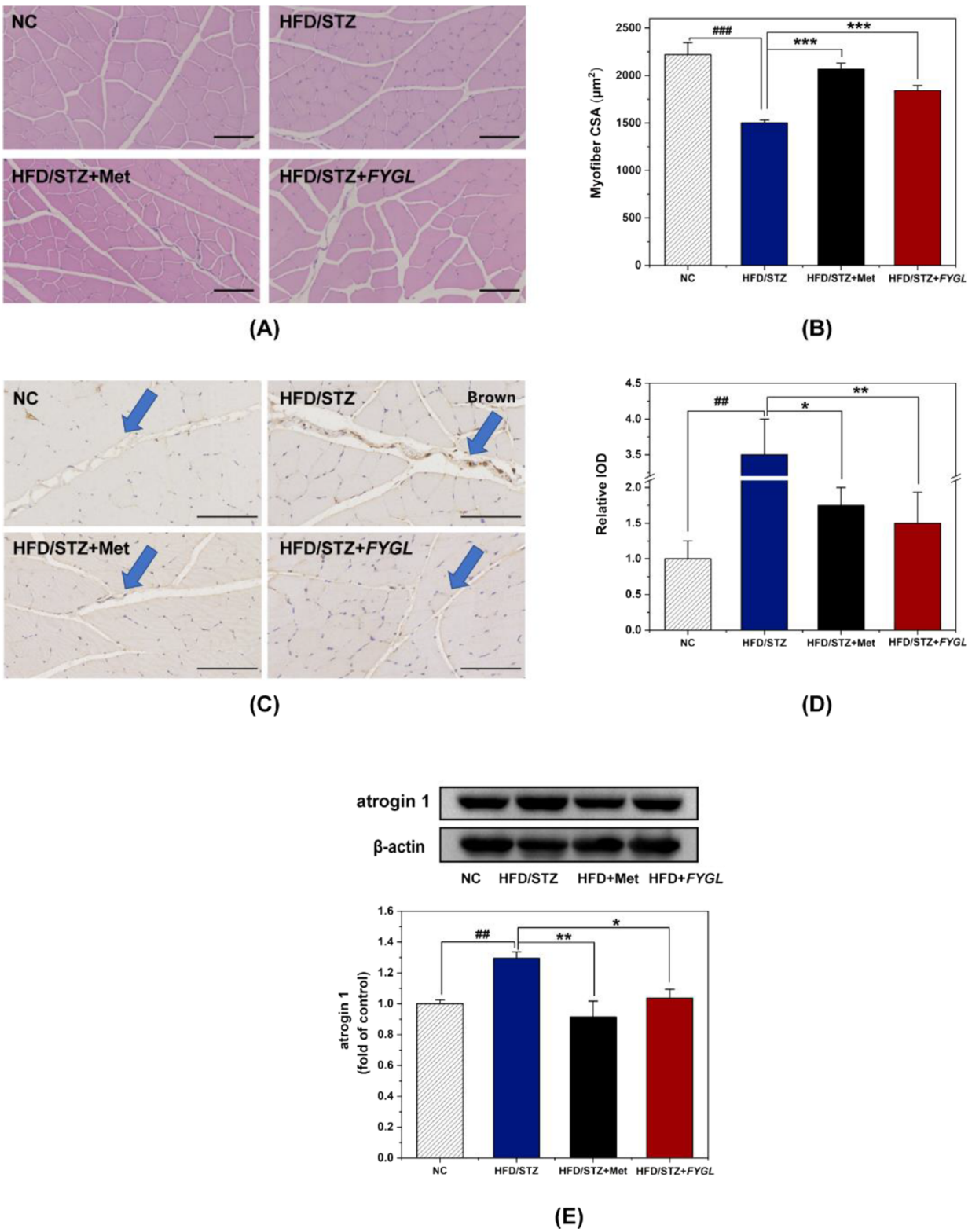

Figure 2. *FYGL* prevented skeletal muscle loss in HFD/STZ-induced T2D rats. (A) Paraffin sections of TA muscle tissue were stained with H&E and observed under a NanoZoomer 2.0-HT. Scale bar = 100 μm. (B) CSA of muscle fibers was measured via Image J software (n = 6). (C) TA muscle tissue was immunohistochemically stained with antibodies against MSTN and observed via NanoZoomer 2.0-HT. The brown color indicates MSTN expression (highlighted with blue arrows). Scale bar = 100 μm.(D) MSTN expression was quantified by IOD using Image J software (n = 6). (E) *Atrogin 1* protein levels in the TA muscle tissue were measured via Western blotting (n = 3). All values are expressed as mean ± SEM. $^{\#\#}P < 0.01$, $^{\#\#\#}P < 0.001$ vs NC. $^{*}P < 0.05$, $^{**}P < 0.01$, $^{***}P < 0.001$ vs HFD/STZ.

muscle atrophy. In this study, the expression of *atrogin 1* in TA muscle was analyzed by Western blotting. *Atrogin 1* expression was significantly increased in HFD/STZ rats, where *FYGL* treatment reversed this change (Figure 2E), indicating that

https://doi.org/10.1021/acsomega.3c03513
ACS Omega 2023, 8, 30359−30373

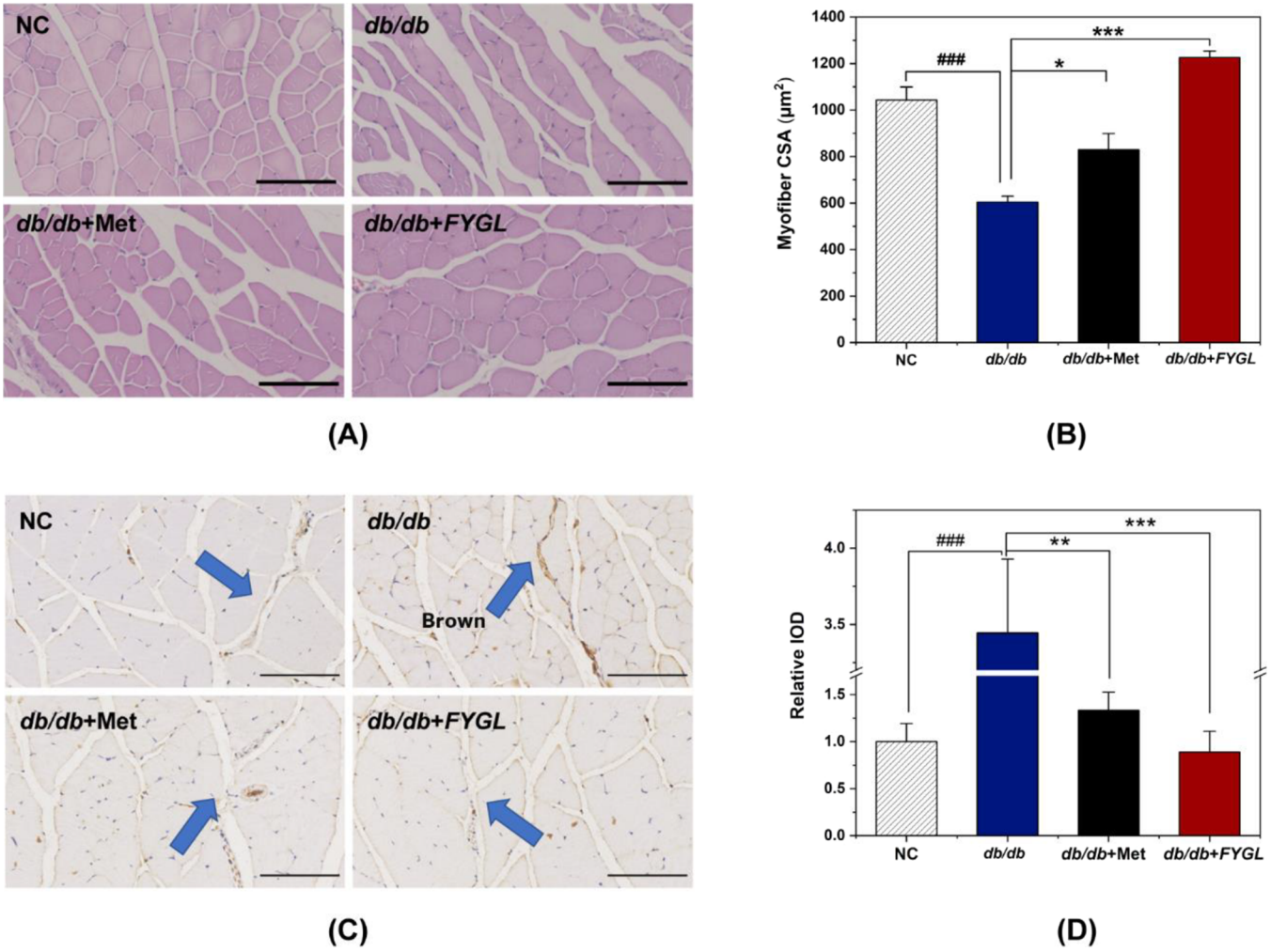

Figure 3. *FYGL* mitigated muscle atrophy in genetically induced T2D mice (*db/db* mice). (A) Paraffin sections of quadriceps muscle tissue were stained with H&E and observed under a NanoZoomer 2.0-HT. Scale bar = 100 μm. (B) CSA of muscle fibers was measured via Image J software (n = 6). (C) Quadriceps muscle tissue was immunohistochemically stained with antibodies against MSTN and observed using the NanoZoomer 2.0-HT. Scale bar = 100 μm. (D) MSTN expression was quantified by IOD using Image J software (n = 6). All values are expressed as mean ± SEM. $^{###}P < 0.001$ vs NC. $^{*}P < 0.05$, $^{**}P < 0.01$, $^{***}P < 0.001$ vs *db/db*.

FYGL down-regulated the expression of *atrogin 1*. Taken together, these results suggest that *FYGL* ameliorated muscle atrophy in HFD/STZ rats.

2.2. *FYGL* Mitigated Muscle Atrophy in Genetically Induced T2D Mice. The effects of *FYGL* on muscle atrophy in a genetically induced T2D mouse model was also investigated. Eight-week old male *db/db* mice were orally administrated *FYGL* or saline for 8 weeks. Male *db/m* mice were used as the normal group (NC mice). Basic metabolic data of *db/db* mice have been studied and published previously[29] as shown in Figure S8. In this study, the quadriceps muscle of the mice was dissected, and the quadriceps muscle sections were stained with H&E to show the inhibitory effects of *FYGL* on muscle atrophy in *db/db* mice. The CSA of the muscle fibers in *db/db* mice was reduced by 42% ($P < 0.001$) compared with the NC group. The observed decrease in the CSA of muscle fibers in *db/db* mice (32%) was more remarkable than in the HFD/STZ rats (42%). This reduction was reversed to normal levels by *FYGL* treatment (Figure 3A,B). Quadriceps muscle sections were immunohistochemically stained to show the expression of MSTN. MSTN protein was up-regulated in *db/db* mice, but this upregulation was inhibited by *FYGL* treatment (Figure 3C,D). These data suggest that *FYGL* mitigated muscle atrophy in *db/db* mice, which is consistent with the observed effects of *FYGL* in HFD/STZ rats. Interestingly, the protective effects of Met against muscle atrophy in *db/db* mice were not obvious, and *FYGL* exhibited better preventive function than Met in *db/db* mice.

2.3. Transcriptomic Changes in Diet-Induced T2D Rats and Genetically Induced T2D Mice after *FYGL* Treatment. To better understand the role of *FYGL* in the regulation of skeletal muscle in HFD/STZ rats and *db/db* mice, changes in the gene expression profiles of skeletal muscle upon *FYGL* treatment were analyzed. TA muscle (from rats) and quadriceps muscle (from mice) were harvested for RNA-seq analysis. In total, 782 transcripts were down-regulated and 711 transcripts were up-regulated in HFD/STZ rats treated with *FYGL* compared with those treated with saline, as shown in the volcano plots (Figure 4A). Among the up-regulated genes, *Cdkn1a*, which is essential for cell cycle arrest and beneficial for skeletal muscle differentiation and myogenesis,[30] was significantly up-regulated by *FYGL* treatment. Among the down-regulated genes, *Id2* was reduced upon *FYGL* treatment

https://doi.org/10.1021/acsomega.3c03513
ACS Omega 2023, 8, 30359−30373

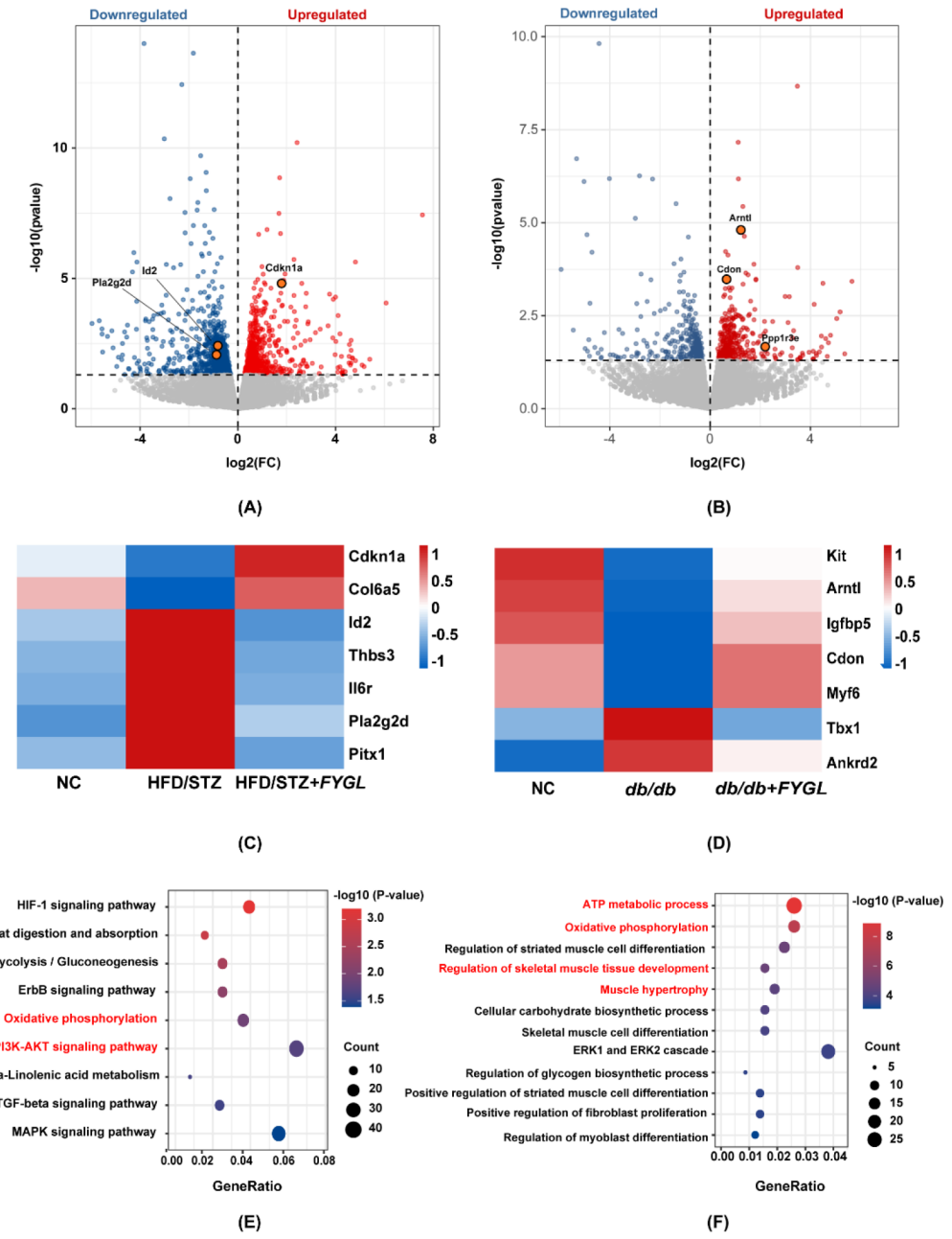

Figure 4. Transcriptomic changes in HFD/STZ rats and *db/db* mice after *FYGL* treatment. (A, B) Volcano plots displaying the DEGs in HFD/STZ rats and *db/db* mice, respectively, following treatment with *FYGL* and compared to non-*FYGL* treatment. The blue and red dots represent the down- and up-regulated genes, respectively. (C, D) Heatmaps of hierarchical clustering displaying DEGs associated with skeletal muscle development in HFD/STZ rats and *db/db* mice following *FYGL* treatment, respectively. (E) Top pathways regulated by *FYGL* in HFD/STZ rats according to KEGG enrichment. (F) Top pathways regulated by *FYGL* in *db/db* mice according to GO enrichment.

in HFD/STZ rats. This gene is known to inhibit skeletal muscle differentiation and cause muscle atrophy by blocking the transcriptional activity of *MyoD*.[31] The regulation of *FYGL* on *Cdkn1a* and *Id2* demonstrates the inhibitory effects of *FYGL* on muscle atrophy in HFD/STZ rats, which is consistent with the immunohistochemistry analysis results. Bioinformatics analyses were conducted to determine the implications of the observed gene expression alterations. Genes associated with skeletal muscle development are displayed in the heatmap by hierarchical clustering, as shown in Figure 4C. *FYGL* reversed the changes in gene expression induced in HFD/STZ rats.

KEGG enrichment analysis was performed to define signaling pathways in HFD/STZ rats affected by *FYGL*, which suggested that the genes involved in oxidative phosphorylation and the PI3K-AKT signaling pathway were differently expressed between saline- and *FYGL*-treated HFD/STZ rats (Figure 4E). It has been reported that the PI3K-AKT pathway facilitates protein synthesis and inhibits proteolysis, thus inducing muscle growth.[32,33] Our results indicated that *FYGL* regulated the process of muscle growth and oxidative phosphorylation in HFD/STZ rats.

FYGL down-regulated 332 genes and up-regulated 371 genes in *db/db* mice compared with *db/db* mice treated with saline. It was noted that *CDON* and *ppp1r3e* were significantly

https://doi.org/10.1021/acsomega.3c03513
ACS Omega 2023, 8, 30359−30373

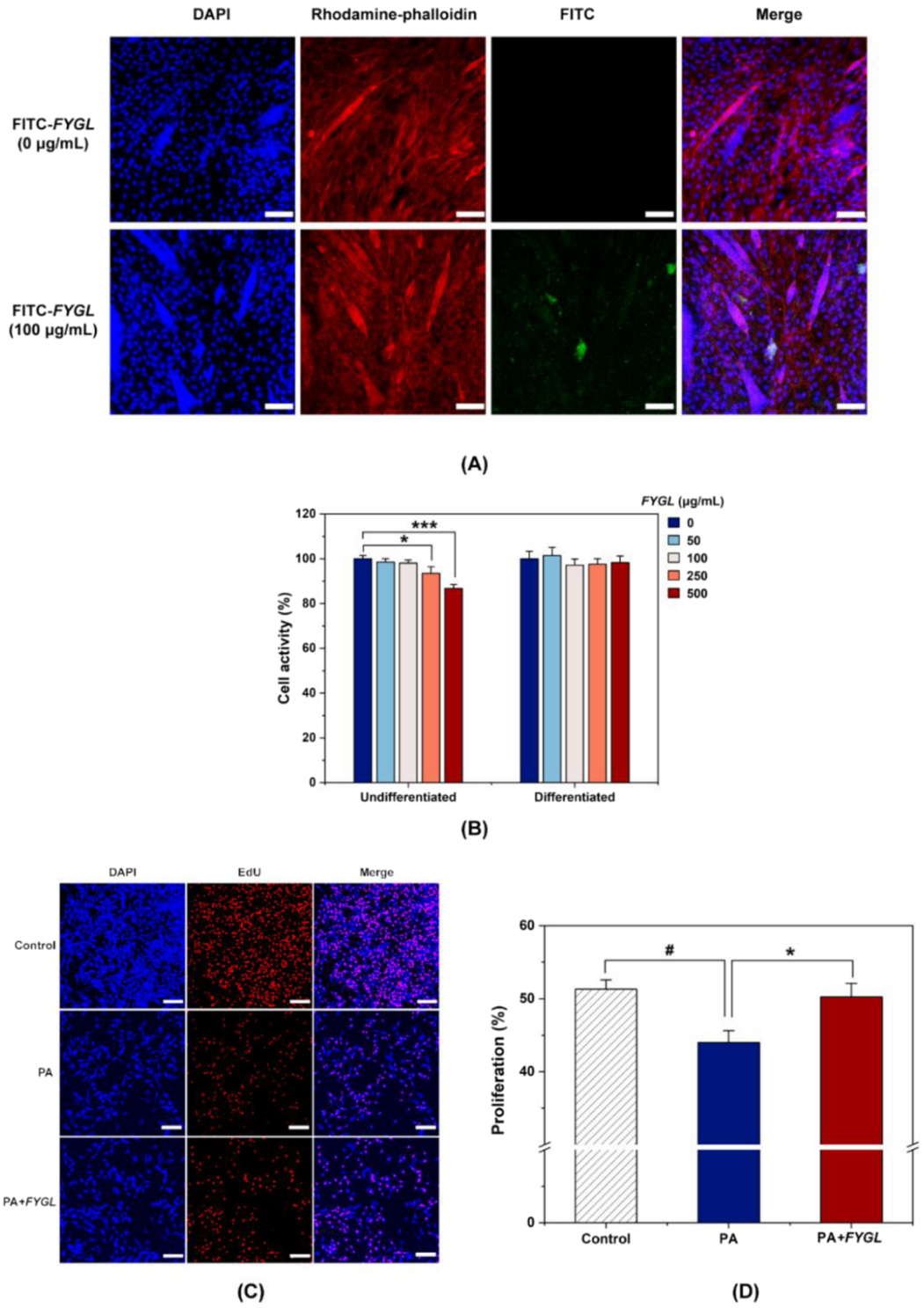

Figure 5. *FYGL* enhanced the proliferation of palmitate-induced C2C12 myoblasts. (A) Absorption of *FYGL* in C2C12 myotubes was observed under a laser confocal microscope. Scale bar = 100 μm. (B) C2C12 myoblasts and fully differentiated myotubes were incubated with *FYGL* for 24 h, and the effect of *FYGL* on cell viability was measured by the cell counting kit-8 (CCK-8) assay (n = 6). (C) C2C12 myoblasts were treated with 200 μM palmitate and 200 μg/mL *FYGL* for 24 h. Cell proliferation was measured with the EdU assay. (D) Proliferation rate was calculated by the ratio of the number of nuclei undergoing DNA replication to the total number of nuclei in the image using Image J software (n = 3). Data are represented as mean ± SEM. $^{\#}P < 0.05$ vs control. $^{*}P < 0.05$ vs PA.

up-regulated (Figure 4B). CDON (cell adhesion molecule-related/down-regulated by oncogenes) is a positive regulator of skeletal myogenesis.[34] The protein encoded by *ppp1r3e* plays a positive role in the regulation of glycogen biosynthetic processes.[35] The DEGs related to skeletal muscle development are displayed in the heatmap by hierarchical clustering. These data demonstrated that *FYGL* reversed the observed changes in gene expression in *db/db* mice compared with NC mice (Figure 4D). KEGG enrichment analysis suggested that genes associated with oxidative phosphorylation were significantly

https://doi.org/10.1021/acsomega.3c03513
ACS Omega 2023, 8, 30359−30373

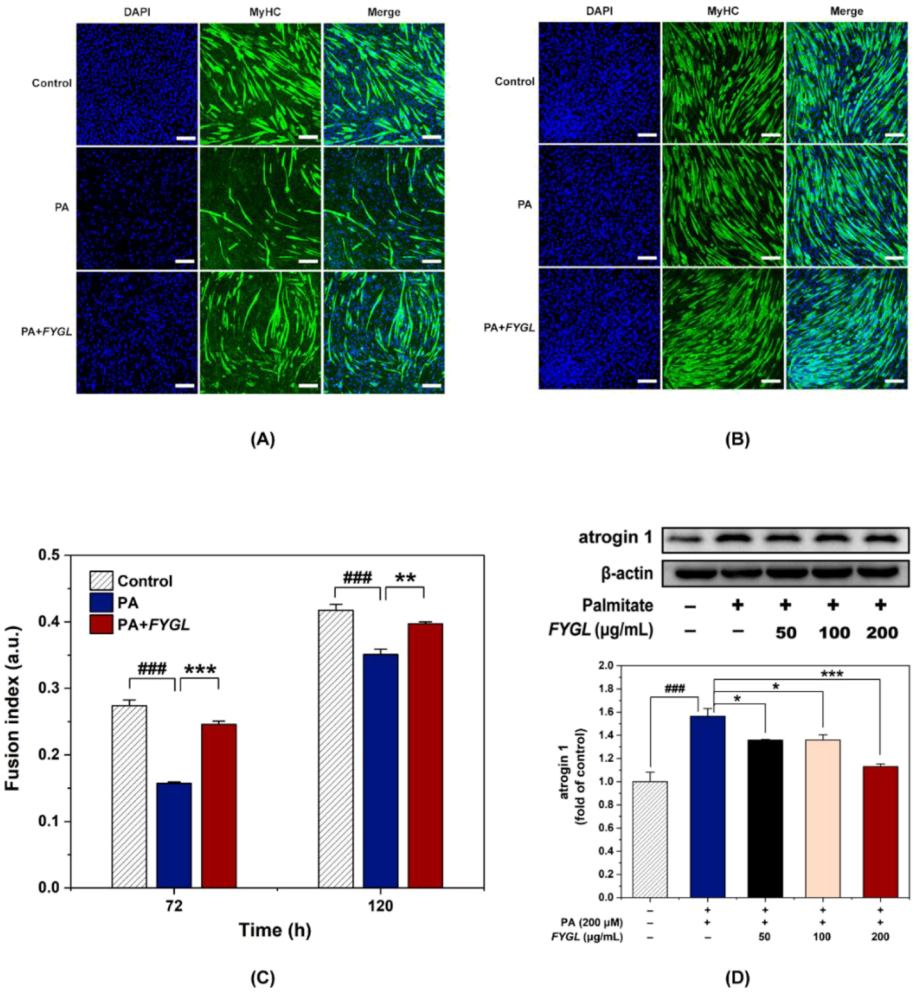

Figure 6. *FYGL* stimulated myotube formation in palmitate-induced C2C12 cells. (A,B) show the myotube formation in C2C12 cells treated with 200 μM palmitate and 200 μg/mL *FYGL* for 24 h on day 3 and day 5 of cell differentiation, respectively. Scale bar = 100 μm. (C) Fusion index was calculated using the ratio of the number of nuclei in C2C12 myotubes to the total number of nuclei in the image (n = 3). (D) On day 5 of cell differentiation, C2C12 myotubes were treated with 200 μM palmitate plus 200 μg/mL FYGL for 24 h, and the protein level of *atrogin 1* in C2C12 cells was measured using Western blotting (n = 3). Data are represented as mean ± SEM. $^{###}P < 0.001$ vs control. $^{*}P < 0.05$, $^{**}P < 0.01$, $^{***}P < 0.001$ vs PA.

enriched (Figure S10). GO enrichment analysis showed that in addition to oxidative phosphorylation, genes associated with ATP metabolic processes, skeletal muscle tissue development, and muscle hypertrophy were differently expressed between saline- and *FYGL*-treated *db/db* mice (Figure 4F). It was noted that the genes related to oxidative phosphorylation in both HFD/STZ rats and *db/db* mice treated with *FYGL* were expressed significantly differently from those without *FYGL* treatment. Oxidative phosphorylation is closely associated with ATP synthesis and oxidative metabolism.[36] Therefore, the regulation of oxidative metabolism is a potential mechanism underlying the inhibitory effects of *FYGL* on muscle atrophy in T2D.

2.4. *FYGL* Promoted Cell Proliferation in Palmitate-Induced C2C12 Cells. A series of experiments were conducted in palmitate-induced C2C12 cells to explore the mechanisms underlying the inhibitory effects of *FYGL* on muscle atrophy in T2D. First, to verify that *FYGL* is absorbed by C2C12 cells, fully differentiated C2C12 myotubes were incubated with 200 μg/mL fluorescein isothiocyanate-labeled *FYGL* (FITC-*FYGL*) for 4 h. As shown in Figure 5A, green FITC fluorescence was observed in C2C12 myotubes incubated with FITC-*FYGL*, while no green fluorescence was observed in myotubes without *FYGL* incubation. This suggested that *FYGL* was effectively absorbed by C2C12 myotubes.

Then, the effect of *FYGL* on cell viability was evaluated using the CCK-8 kit. Although a slight decrease in cell viability was observed in undifferentiated C2C12 myoblasts incubated with 250 and 500 μg/mL *FYGL*, the cell viability remained above 80% (Figure 5B). In fully differentiated C2C12 myotubes, incubation with *FYGL* (0−500 μg/mL) did not result in apparent cytotoxicity (Figure 5B). To investigate the effect of *FYGL* on the proliferation of palmitate-induced C2C12 cells, the EdU incorporation assay was performed. Results showed that cell proliferation was significantly inhibited after 24 h treatment with palmitate. In addition, coincubation with *FYGL* partially increased the mitotic activity of myoblasts, demonstrating that *FYGL* promoted cell proliferation in palmitate-induced C2C12 myoblasts (Figure 5C,D). The promotion of cell proliferation enhanced the efficacy of *FYGL* to induce skeletal myogenesis since myotubes are formed by cell fusion.

https://doi.org/10.1021/acsomega.3c03513
ACS Omega 2023, 8, 30359−30373

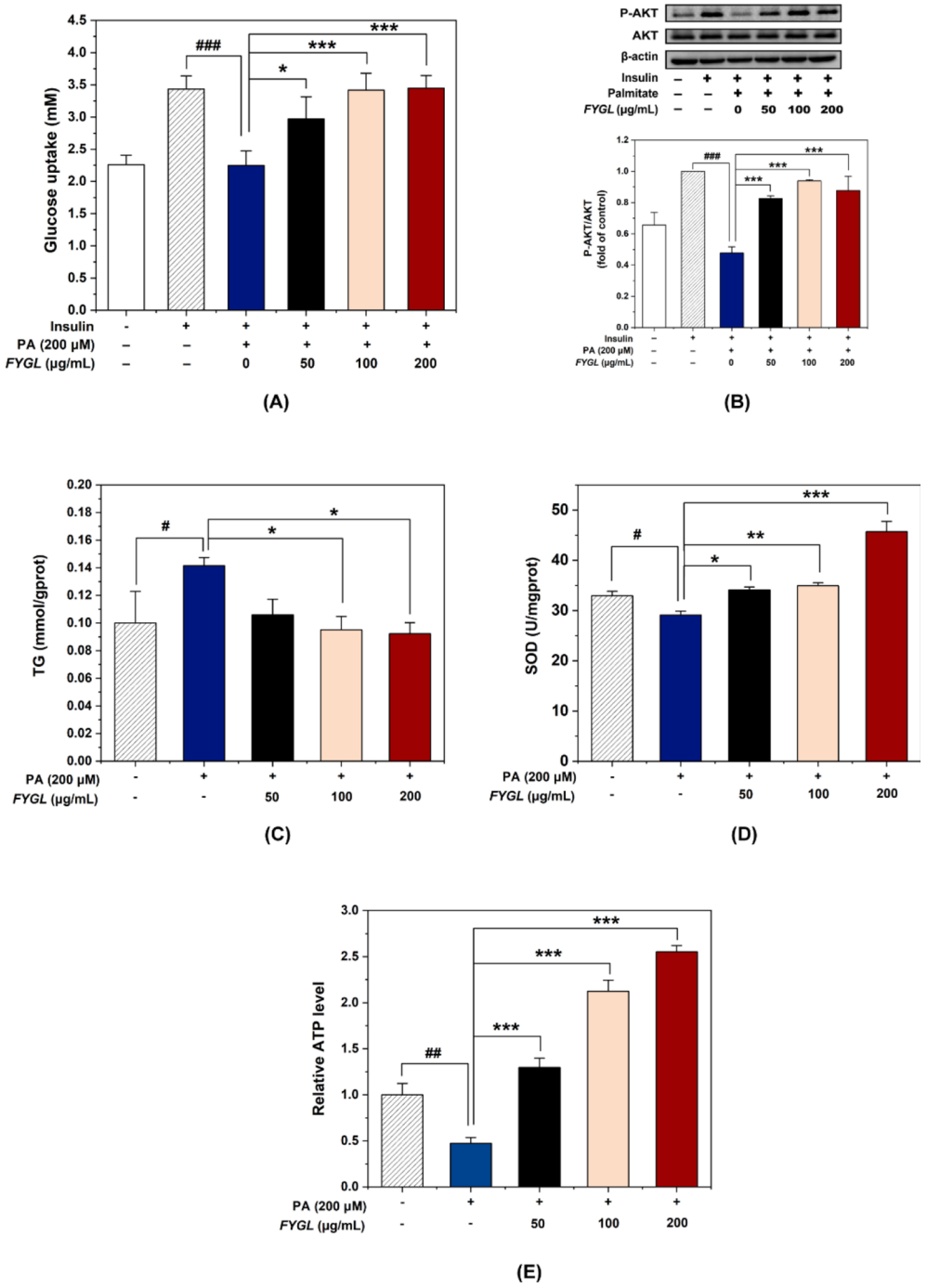

Figure 7. *FYGL* regulated the metabolic indicators in palmitate-induced C2C12 cells. (A) Effect of *FYGL* on glucose uptake levels in fully differentiated C2C12 myotubes treated with 200 μM palmitate and 200 μg/mL *FYGL* for 24 h. (B) Effects of *FYGL* on AKT phosphorylation in palmitate-induced C2C12 cells analyzed by Western blotting. (C–E) Effects of *FYGL* on TG, SOD, and ATP production in palmitate-induced C2C12 cells. All values are expressed as mean ± SEM. $^{\#}P < 0.05$, $^{\#\#}P < 0.01$, $^{\#\#\#}P < 0.001$ vs control. $^{*}P < 0.05$, $^{**}P < 0.01$, $^{***}P < 0.001$ vs PA.

2.5. *FYGL* Ameliorated Muscle Atrophy in Palmitate-Induced C2C12 Cells. To investigate the effect of *FYGL* on muscle atrophy in palmitate-induced C2C12 cells, the expression of the myogenic marker myosin heavy chain (MyHC)[37,38] was observed on day3 and day 5 of cell differentiation by immunofluorescence staining. On day3, approximately 50% of the C2C12 myoblasts had fused into long and multinucleated fibers in the NC group (cells without any treatment). However, palmitate treatment decreased MyHC expression by 43% ($P < 0.001$) and reduced myotube formation. However, *FYGL* treatment significantly minimized the loss of MyHC expression and promoted myotube formation (Figure 6A,C). On day five, almost all myoblasts had fused into myotubes. Palmitate treatment decreased MyHC expression by 17% ($P < 0.001$) and reduced myotube formation (Figure 6B,C), whereas *FYGL* treatment increased the expression of MyHC and stimulated myotube formation. These data imply that *FYGL* efficiently promoted the expression of the myogenic marker, thus protecting C2C12 cells from palmitate-induced muscle atrophy.

https://doi.org/10.1021/acsomega.3c03513
ACS Omega 2023, 8, 30359−30373

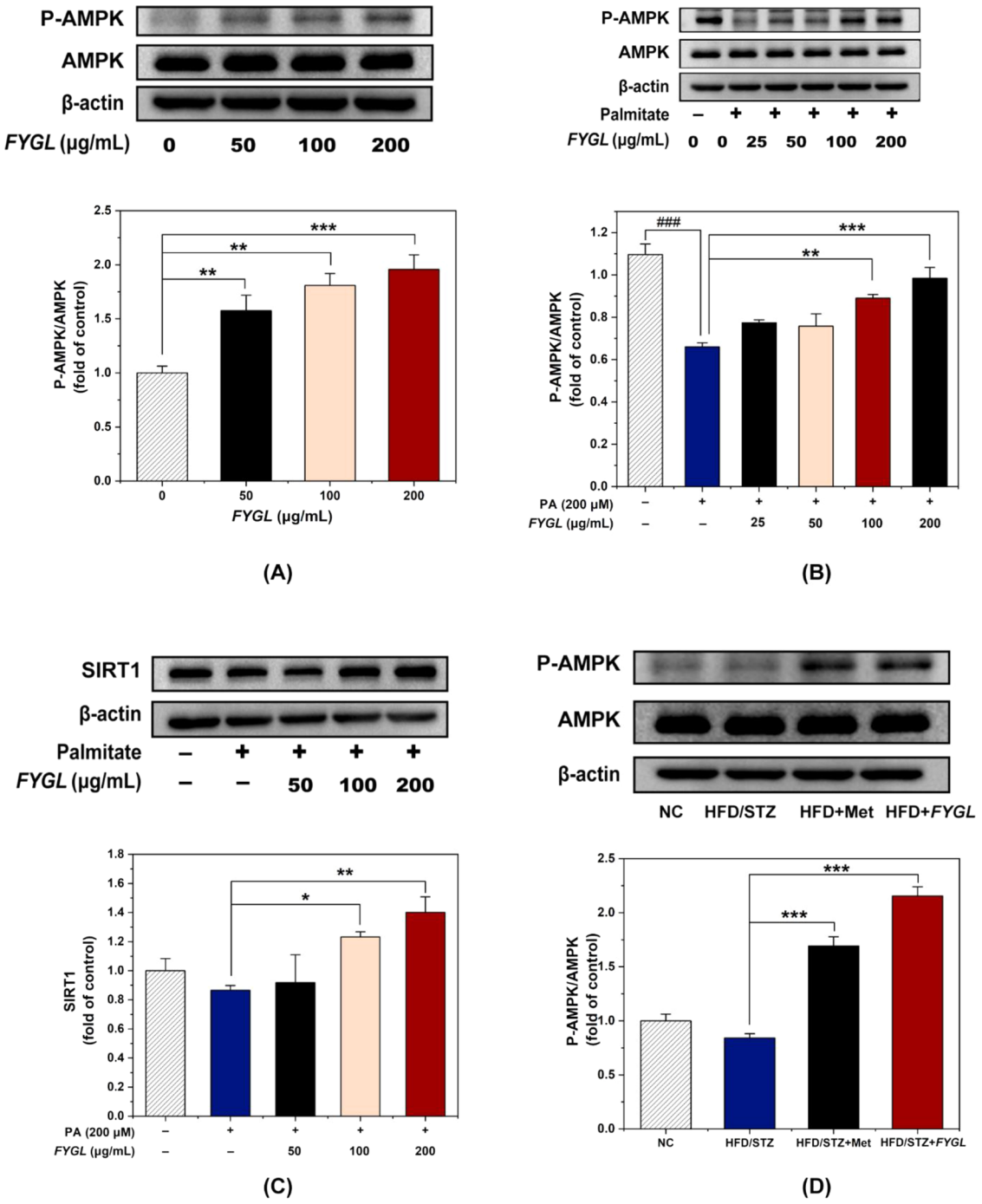

Figure 8. *FYGL* ameliorated muscle atrophy in T2D via activation of the AMPK/SIRT1 signaling pathway. (A) AMPK phosphorylation in C2C12 myotubes treated with different concentrations of *FYGL* for 24 h. (B) AMPK phosphorylation in C2C12 myotubes treated with 200 μM palmitate and 200 μg/mL *FYGL* for 24 h. (C) SIRT1 expression in C2C12 myotubes treated with 200 μM palmitate and 200 μg/mL *FYGL* for 24 h. (D) AMPK phosphorylation in the TA muscle tissue from HFD/STZ rats. All values are expressed as mean ± SEM, $n = 3$. $^{\#\#\#}P < 0.001$ vs control, $^{*}P < 0.05$, $^{**}P < 0.01$, $^{***}P < 0.001$ vs control, PA, or HFD/STZ.

To further verify the inhibitory effect of *FYGL* on muscle atrophy in C2C12 cells, the expression of *atrogin 1*, a marker of muscle atrophy, was detected by Western blotting. The expression of *atrogin 1* was increased in palmitate-induced C2C12 cells, where *FYGL* reversed this change (Figure 6D). This indicates that *FYGL* down-regulated the expression of *atrogin 1* in palmitate-induced C2C12 cells, which is consistent with the findings in HFD/S TZ rats. Taken together, these results suggest that *FYGL* ameliorated muscle atrophy in palmitate-induced C2C12 cells.

2.6. *FYGL* Ameliorated Muscle Atrophy in T2D via the AMPK/SIRT1 Pathway. To understand the underlying mechanisms of *FYGL* amelioration of muscle atrophy in palmitate-induced C2C12 cells, we measured indicators closely related to glucose and lipid metabolism, energy metabolism, and inflammatory responses such as glucose uptake, triglyceride (TG), superoxide dismutase (SOD), and ATP.

https://doi.org/10.1021/acsomega.3c03513
ACS Omega 2023, 8, 30359−30373

Glucose uptake was inhibited in palmitate-induced C2C12 cells, where *FYGL* (0−200 μg/mL) stimulated glucose uptake in a concentration-dependent manner (Figure 7A). AKT, a positive regulator in glucose uptake,[39] is involved in the phosphoinositide 3-kinase (PI3K)-AKT-mammalian target of rapamycin (mTOR) pathway. This pathway stimulates protein synthesis and inhibits protein degradation in the skeletal muscle.[32] Therefore, the effect of *FYGL* on AKT was investigated. As shown in Figure 7B, palmitate suppressed phosphorylation of AKT (Ser473) where *FYGL* significantly enhanced the phosphorylation of AKT in palmitate-induced C2C12 cells. Therefore, *FYGL* may ameliorate muscle atrophy via the activation of AKT. A reduction in TGs was observed after 24 h treatment with palmitate, which was reversed by *FYGL* (100−200 μg/mL) (Figure 7C). SOD activity was slightly reduced in palmitate-induced C2C12 cells and elevated by the cotreatment of *FYGL* in a concentration-dependent manner (Figure 7D). These results indicate that *FYGL* promoted glucose uptake and reduced lipid accumulation in palmitate-induced C2C12 cells and exerted anti-inflammatory effects.

In addition, it was noted that palmitate treatment led to a significant decrease in ATP production in C2C12 cells, whereas *FYGL* stimulated ATP production in a concentration-dependent manner (Figure 7E). The ATP level in cells incubated with *FYGL* (200 μg/mL) increased by 155% ($P < 0.001$) compared with the NC group. This result was consistent with the transcriptome analysis finding that *db/db* mice treated with *FYGL* exhibited differential expression of genes implicated in ATP metabolic processes and oxidative phosphorylation compared with mice not receiving *FYGL* treatment (Figure 4F).

The RNA-seq analysis and ATP measurement results showed that *FYGL* significantly affected energy metabolism in the skeletal muscle. AMPK is a master regulator of mitochondrial biogenesis and energy metabolism.[9] As shown in Figure 8A, when fully differentiated C2C12 myotubes were incubated with different concentrations of *FYGL* for 24 h, the phosphorylation of AMPK increased in a dose-dependent manner. Notably, *FYGL* (200 μg/mL) promoted the phosphorylation of AMPK by 96% ($P < 0.001$) compared with the NC group. Increased phosphorylation of AMPK was also observed in palmitate-induced C2C12 myotubes (Figure 8B). Phosphorylated AMPK (Thr172) subsequently activated its downstream protein SIRT1 (Figure 8C), which suppressed the overexpression of *atrogin 1* (Figure 6D) and prevented muscle atrophy in palmitate-induced C2C12 myotubes. Our data showed that palmitate treatment has no effect on SIRT1 expression compared to the NC group. The reason may be that the effect of palmitate on SIRT1 expression is related to the treatment time and concentration of palmitate. It is reported that 12-hour treatment of palmitate (500 μM) showed no effect on SIRT1 expression.[40] Moreover, the activation of AMPK was also observed in HFD/STZ rats treated with *FYGL* or Met compared with those treated with saline (Figure 8D). These results suggest that *FYGL* may ameliorate muscle atrophy in T2D via activation of the AMPK/SIRT1 signaling pathway.

3. DISCUSSION

Emerging evidence has shown that muscle atrophy is a comorbidity of T2D, resulting in physical disability and reduced quality of life.[3,41] However, current treatments for diabetes-induced muscle atrophy are limited and result in unwanted side effects. Yang et al. demonstrated that *FYGL* effectively alleviated skeletal muscle insulin resistance in T2D mice.[19] Teng et al. proved that in mice, *FYGL* was absorbed through the small intestine and remained in the body for 6 h, providing the necessary conditions for *FYGL* treatment efficacy.[42] The median lethal dose (LD_{50}) of *FYGL* in mice is 6 g/kg, indicating that *FYGL* has a high level of safety.[16] In this work, *FYGL* was demonstrated capable of ameliorating T2D-induced muscle atrophy both in vitro and in vivo through promoting oxidative metabolism and activating the AMPK/SIRT1 pathway, with few side effects. These data suggest there may be therapeutic benefits of *FYGL* treatment in improving muscle dysfunction in T2D.

In the current study, several pieces of evidence have demonstrated the inhibitory effects of *FYGL* on diabetes induced muscle atrophy. Histopathological analysis showed that oral administration of *FYGL* increased the muscle fiber CSA (Figures 2B and 3B) and inhibited the overexpression of myostatin (Figures 2D and 3D), a negative regulator of muscle mass, in both diet-induced T2D rats (HFD/STZ rats) and genetically induced T2D mice (*db/db* mice). These results are consistent with reports of other natural compounds, such as resveratrol derived from whole grains,[43] quercetin,[44] and ghrelin,[45] which have been shown to contribute to the enhancement of muscle mass in mouse models. Besides, it was found that *FYGL* significantly suppressed the expression of *atrogin 1*, a marker of muscle atrophy,[4] in HFD/STZ rats (Figure 2E). It has been reported that suppressing the overexpression of *atrogin 1* in the skeletal muscle could prevent dexamethasone-induced muscle atrophy.[12] RNA-seq analysis results showed that *FYGL* also up-regulated myogenic genes and down-regulated muscle atrophic genes in both HFD/STZ rats (Figure 4A) and *db/db* mice (Figure 4B). These results demonstrate that *FYGL* is capable of ameliorating muscle atrophy in different models of T2D. Promisingly, rats and mice treated with *FYGL* did not exhibit adverse reactions. This could be attributed to the fact that *FYGL* is a proteoglycan, which typically exhibits lower toxicity compared to small-molecule drugs.

Our data indicate that *FYGL* affected the expression of genes related to oxidative phosphorylation in the skeletal muscle of both diet-induced T2D rats and genetically induced T2D mice (Figure 4E,F). Oxidative phosphorylation is closely associated with ATP synthesis and mitochondrial biogenesis.[36] Research has shown that some therapeutic agents for muscle atrophy exhibit beneficial effects on muscle mass by improving mitochondrial function in the skeletal muscle.[10,46,47] For example, atomoxetine ameliorated dexamethasone-induced atrophy by promoting mitochondrial biogenesis.[48] Therefore, promoting mitochondrial biogenesis and oxidative metabolism may be a potential mechanism underlying the inhibitory effects of *FYGL* on T2D-induced muscle atrophy in T2D. Palmitate-induced C2C12 cells were used to validate this hypothesis. Our data showed that *FYGL* stimulated ATP production and activated AMPK in a concentration-dependent manner in palmitate-induced C2C12 cells (Figures 7E and 8A). AMPK is highly involved in the regulation of energy balance and mitochondrial biogenesis. It is reported that AMPK activates SIRT1 and suppresses the expression of *atrogin 1*, thus reducing the degradation of muscle proteins and preventing muscle loss.[11,49] In our study, we observed that treatment of *FYGL* promoted the phosphorylation and subsequently

https://doi.org/10.1021/acsomega.3c03513
ACS Omega 2023, 8, 30359−30373

activated downstream protein SIRT1 in palmitate-induced C2C12 cells (Figure 8C). Besides, the elevated phosphorylation of AMPK was also observed in HFD/STZ rats treated with *FYGL* (Figure 8D). Taken together, these data suggest that *FYGL* may prevent T2D-related muscle atrophy by promoting oxidative metabolism and activating the AMPK/SIRT1 signaling pathway.

AMPK is comprised of a catalytic α subunit and regulatory β and γ subunits.[50] The activation of AMPK requires the binding of AMPK activators to the CBM-KD (carbohydrate binding module-kinase domain) interface formed by the kinase domain of the α subunit and the carbohydrate binding module of the β subunits.[51,52] A769662 was the first reported AMPK activator[53] and was shown to bind to the CBM-KD interface via hydrogen bonds formed by the interaction between the hydroxyl of A769662 and the CBM-KD interface.[54] Research has shown that many reported AMPK activators such as astaxanthin,[55] quercetin,[56] and canagliflozin[57] contain hydroxyl groups, indicating that hydroxyl groups are beneficial to their binding to the CBM-KD interface. Moreover, it has been reported that the CBM motif tends to bind carbohydrates, for example, polysaccharides.[58] Therefore, the function of *FYGL* in activating AMPK may be attributed to its abundant hydroxyl groups in the polysaccharide moieties.[16]

The PI3K-AKT−mTOR pathway also plays an important role in regulating skeletal muscle growth, and activation of PI3K/AKT signaling can stimulate protein synthesis and inhibit protein degradation.[59] Our data also showed that *FYGL* affected the expression of genes associated with the PI3K/AKT signaling pathway in HFD/STZ rats (Figure 4E). *FYGL* also activated AKT in palmitate-induced C2C12 cells (Figure 7B), indicating that the protective effect of *FYGL* on T2D related muscle atrophy is closely linked to the PI3K/AKT signaling pathway. Additionally, inflammation initiated by prolonged overnutrition in diabetics promotes muscle atrophy, and NF-κB is crucial to the regulation of inflammatory responses. The increase in SOD activity (Figure 7B) in palmitate-induced C2C12 cells by *FYGL* treatment suggests that *FYGL* exerts anti-inflammatory effects, and NF-κB may also be involved in the mechanism behind the effects of *FYGL* on muscle atrophy. Furthermore, in addition to stimulating protein synthesis and reducing protein degradation to expand the size of muscle fibers,[60] muscle mass can also be increased by promoting the proliferation of muscle cells to increase the number of muscle fibers since they are formed by muscle cell fusion.[3,37] Our data showed that *FYGL* slightly promoted proliferation and myotube formation in palmitate-induced C2C12 cells (Figure 5D).

The present study indicates that *FYGL* may ameliorate T2D-induced muscle atrophy mainly in two potential ways. *FYGL* promoted muscle cell proliferation to increase the number of muscle fibers. *FYGL* also activated the AMPK/SIRT1 and PI3K/AKT signaling pathways to increase protein synthesis and inhibit protein degradation, thus expanding the size of pre-existing muscle fibers. Further work needs to be undertaken to confirm the biological effects of *FYGL* in the human skeletal muscle.

4. CONCLUSIONS

FYGL is a proteoglycan that was first extracted from *Ganoderma lucidum* by our group. In the present study, the inhibitory effects of *FYGL* on muscle atrophy in T2D were identified in diet-induced T2D rats and genetically induced T2D mice. Promisingly, mice and rats treated with *FYGL* did not exhibit any adverse reactions. The underlying molecular mechanisms studied in palmitate-induced C2C12 muscle cells revealed that *FYGL* ameliorated T2D-related muscle atrophy by significantly activating AMPK and its downstream protein SIRT1, thus promoting oxidative metabolism. The function of *FYGL* in activating AMPK may be attributed to the abundant hydroxyl groups in *FYGL*, which enables *FYGL* to bind AMPK via hydrogen bonding. Taken together, these results suggest that *FYGL* is a promising functional food ingredient for ameliorating T2D-induced muscle atrophy, with few side effects. Further work will be conducted to confirm the safety and biological effects of *FYGL* in clinical phase I and II studies.

5. MATERIALS AND METHODS

5.1. Reagents. Fruiting bodies of *Ganoderma lucidum* grown in Northeast China were purchased from Leiyunshang Pharmaceutical Co., Ltd. (Shanghai, China). STZ was purchased from Yeasen Biotechnology Co., Ltd. (Shanghai, China).

5.2. *FYGL* Preparation. The fruiting bodies of *Ganoderma lucidum* were dried, milled, and defatted with boiling ethanol (95%) for 30 min. Then, the ethanol insoluble residues were dried and decocted with boiling water for 2 h, and the solid residue was extracted with ammonia solution at room temperature for 24 h. The alkali extract was neutralized, concentrated, dialyzed, lyophilized, and further purified via Sephadex G-75 column chromatography using 0.5 M NaCl solution as the eluent. The phenol−sulfuric acid method was used to characterize the elutes with ultraviolet (UV) absorption at a wavelength of 490 nm, and *FYGL* was obtained by lyophilization for the following experiments. The content of *FYGL* in *Ganoderma lucidum* is about 1%.[61]

5.3. Animal Models. To investigate the effects of *FYGL* on skeletal muscle atrophy in diabetic animals, two different models of T2D were established. All animal trials were performed according to protocols approved by the Institutional Animal Care and Use Committee of Fudan University.

For the diet-induced T2D model, 4-week old male SD rats were purchased from Shanghai Slake Experimental Animal Co., Ltd. (Shanghai, China). After acclimatization for1 week, rats were randomly divided into the normal group and the model group. Rats of the normal group (NC, n = 14) were fed a normal diet. Rats of the model group were fed a HFD consisting of 10% fat, 2% cholesterol, and 1% bile salt for 4 weeks. Then, the rats that were fed HFD were given a single injection of STZ (40 mg/kg in 0.1 M citric acid/sodium citrate buffer, pH = 4.3). After 1 week, the fasting blood glucose (FBG) levels were examined by the blood glucose test strip, and rats with FBG levels <11 mmol/L were treated again with STZ. Finally, rats with FBG levels >11.0 mmol/L were considered diabetic. The HFD/STZ-induced rats were randomly divided into three groups (n = 14 per group): HFD/STZ group (saline), HFD/STZ plus Met group (200 mg/kg/day), and HFD/STZ plus *FYGL* group (300 mg/kg/day). Met was used as a positive control. Rats were orally administrated *FYGL*, Met, or saline for 4 weeks. The body weight of rats was recorded weekly.

For the genetically induced T2D model, 4-week old male BKS-*db/db* mice and heterozygous male *db/m* mice were purchased from GemPharmatech Co., Ltd. (Nanjing, China). At 8 weeks of age, hyperglycemia was noted in *db/db* mice. Then, *db/db* mice were randomly divided into three groups (n

https://doi.org/10.1021/acsomega.3c03513
ACS Omega 2023, 8, 30359−30373

= 12 per group): *db/db* group (saline), *db/db* plus Met group (225 mg/kg/day), and *db/db* plus *FYGL* group (450 mg/kg/day). Male *db/db* mice were orally administrated *FYGL*, Met, or saline for 8 weeks. Male *db/m* mice were used as the normal group (NC, n = 12). The body weight of mice was recorded weekly.

5.4. Histological Staining and Immunohistochemistry of the Skeletal Muscle. The TA muscle was harvested from the rats, and the quadriceps muscle was harvested from the mice. Then, the tissues were embedded in paraffin and sectioned at a 5 μm thickness. Muscle sections were stained with H&E and observed using a NanoZoomer 2.0-HT (Hammatsu, Japan). The CSA of the muscle fibers was measured via Image J software.

Muscle sections were immunohistochemically stained to analyze the expression of MSTN. The slides were then dewaxed, and the antigens were retrieved in citrate buffer for 20 min. Endogenous peroxidase activity was blocked, and the slides were incubated with phosphate-buffered saline (PBS) containing 5% bovine serum albumin (BSA; Yeasen Biotechnology, Shanghai, China). Then, the skeletal muscle samples were stained with primary antibodies against MSTN (Abcam, Cambridge, MA, USA) at 4 °C overnight, followed by incubation with a biotin-labeled secondary antibody. Streptavidin-peroxidase reagent 3,3-diaminobenzidine was used as the chromogen. Finally, the muscle sections were counterstained with hematoxylin and observed on a NanoZoomer 2.0-HT. The expression of MSTN was quantified by integrated optical density (IOD) using Image J software.

5.5. RNA Sequencing and Bioinformatics Analysis. Total RNA was extracted from fresh-frozen TA muscle (from rats) and quadriceps muscle (from mice). Libraries of the extracted RNA were prepared using the NEBNext UltraTM RNA Library Prep Kit for Illumina (NEB, USA) following the manufacturer's instructions. Sequencing was done on an Illumina Novaseq platform. Reads were aligned to the reference genome using Hisat2 v2.0.5 and were counted with FeatureCounts v1.5.0-p3. Differential expression analysis was performed with the DESeq2 R package (1.16.1). Genes with an adjusted P value <0.05 and |log2 (FoldChange)| > 0 were regarded as DEGs. GO (gene ontology) enrichment analysis and KEGG (Kyoto Encyclopaedia of Genes and Genomes) enrichment analysis of DEGs were performed using the ClusterProfiler R package to investigate the effect of *FYGL* on gene pathways in skeletal muscle from diabetic mice and rats. The RNA-seq data of the rats and mice were deposited in the NCBI Sequence Read Archive (SRA BioProject ID PRJNA937630 and PRJNA937470, respectively).

5.6. Cell Culture. Mouse myoblast C2C12 cells were obtained from Procell (Wuhan, China) and cultured in DMEM (Gibco, Thermo Fisher Scientific, Waltham, MA, USA) supplemented with 10% fetal bovine serum (Gibco) and 1% penicillin–streptomycin (Gibco). Cells were grown at 37 °C in an incubator with 5% CO_2. When C2C12 cells reached approximately 80% confluence, they were incubated in DMEM with 2% horse serum for 5 days to induce cell differentiation.

5.7. Detection of *FYGL* Absorption in Cells. To detect the absorption of *FYGL* in cells, FITC-labeled *FYGL* was prepared. FITC (Yeasen Biotechnology) was dissolved in DMSO, and water-soluble *FYGL* was dissolved in Na_2CO_3/$NaHCO_3$ buffer. FITC (1 mg/mL) was added into the *FYGL* solution (1 mg/mL) to form FITC-*FYGL*, and the mixture was incubated in the dark at 4 °C for 12 h. Extensive dialysis of the mixture was performed using 1 L of PBS in the dark until the unreacted FITC was removed. Finally, FITC-*FYGL* was obtained. The ultraviolet (UV) spectra of FITC, *FYGL*, and FITC-*FYGL* are shown in Figure S9. FITC has a maximum UV absorption at 495 nm, while *FYGL* is a proteoglycan and has a maximum UV absorption at 280 nm. It can be estimated that the ratio of *FYGL* and FITC in FITC-*FYGL* is 100:117 according to the following equation:[62]

$$\frac{F}{P} = 3.1 \times A_{495}/(A_{280} - 0.31 \times A_{495}) \quad (1)$$

where F and P represent FITC and protein, and A denotes the absorbance. C2C12 myoblasts were seeded at a density of 2×10^5 cells/well in six-well plates, and fully differentiated myotubes were incubated with 100 μg/mL FITC-*FYGL* for 4 h. DAPI (Beyotime, Shanghai, China) and rhodamine phalloidin were used for nuclear and cytoskeleton staining, respectively. The absorption of FITC-*FYGL* in C2C12 myotubes was observed under a laser confocal microscope (C2+; Nikon, Tokyo, Japan).

5.8. Cell Viability Assay. Cell counting kit-8 (CCK-8; Beyotime) was used to evaluate the effect of *FYGL* on cell viability. C2C12 myoblasts were seeded at a density of 1×10^4 cells/well in 96-well plates and maintained for 24 h. Cells were then treated with different concentrations (0, 50, 100, 250, and 500 μg/mL) of *FYGL* for 24 h. Cell viability was determined by incubating the myoblasts with DMEM containing the CCK-8 assay reagent for 4 h. Absorbance of the formed formazan at 450 nm was measured using a microplate reader (Cytation3; Bio Tek, Winooski, VT, USA). To investigate the effect of *FYGL* on the viability of C2C12 myotubes, the cells were seeded at a density of 2×10^5 cells/well in six-well plates and induced to fully differentiate for 5 days. Then, the cells were treated with different concentrations (0, 50, 100, 250, and 500 μg/mL) of *FYGL* for 24 h. After treatment, cell viability was measured using CCK-8 as described above.

5.9. Cell Proliferation Assay. EdU assay (Ribobio, Guangzhou, China) was used to evaluate the effect of *FYGL* on palmitate-induced C2C12 myoblast proliferation. Sodium palmitate (Sigma, St Louis, MO, USA) was conjugated to 2% BSA (fatty acid free; Yeasen Biotechnology, Shanghai, China) dissolved in DMEM, and 200 μM palmitate was prepared. BSA (2%) was used as the control. C2C12 myoblasts were seeded at a density of 5000 cells/well in 48-well plates and maintained for 24 h. Then, the cells were treated with 200 μM palmitate and 200 μg/mL *FYGL* for 24 h. After incubation with 50 μM EdU for 2 h, cells were stained for EDU according to the manufacturer's protocol. Images were captured using a laser confocal microscope (Nikon). Proliferation rate was calculated as the ratio of the number of nuclei undergoing DNA replication to the total number of nuclei in the image.

5.10. Immunofluorescence Staining. C2C12 myoblasts were seeded at a density of 2×10^5 cells/well in six-well plates. On the third and fifth day of cell differentiation, cells were treated with 200 μM palmitate and 200 μg/mL *FYGL* for 24 h. BSA (2%) was used as the control. After treatment, cells were fixed with 4% paraformaldehyde for 10 min and permeabilized with 0.2% Triton X-100 in PBS for 5 min. After blocking with 5% BSA for 30 min, C2C12 cells were incubated with the MyHC antibody (1:100; Santa Cruz Biotechnology, Santa Cruz, CA, USA) for 1 h and then subsequently incubated with the Alexa Fluor 488 (1:500; Beyotime) secondary antibody for 1 h. DAPI (Beyotime; 5 mg/mL) was used for nuclear staining.

https://doi.org/10.1021/acsomega.3c03513
ACS Omega 2023, 8, 30359−30373

Images were captured via a laser confocal microscope (Nikon). The fusion index was calculated as the ratio of the number of nuclei in the C2C12 myotubes to the total number of nuclei in the image.

5.11. Measurement of Glucose Uptake, TG, SOD, and ATP. C2C12 myoblasts were induced to full differentiation for 5 days. Then, cells were treated with 200 μM palmitate and 200 μg/mL *FYGL* for 24 h. After treatment, glucose uptake levels, TG content, and SOD in cells were measured using a glucose kit (Nanjing Jiancheng Bioengineering Institute, Nanjing, China), TGs assay kit (Nanjing Jiancheng Bioengineering Institute), and a total SOD assay kit with WST-8 (Beyotime), respectively, following the manufacturer's directions. Before glucose uptake measurement, cells were stimulated with 100 nM insulin for 10 min.

ATP content was measured using an ATP assay kit (Beyotime). C2C12 cells were seeded at a density of 2×10^5 cells/well in six-well plates and induced to differentiate for 5 days. Fully differentiated C2C12 myotubes were treated with 200 μM palmitate and 200 μg/mL *FYGL* for 24 h. After treatment, cells were lysed, and the whole cell lysates were centrifuged at 12,000 × *g* for 5 min at 4 °C. The supernatants were collected and mixed with ATP detection working solution containing luciferase. Luciferase intensity was detected using a multifunctional microplate reader (Bio Tek). ATP content was normalized to the protein concentration of cells in each well.

5.12. Western Blotting. Muscle tissue was homogenized in lysis buffer (RIPA, Beyotime) containing protease and phosphatase inhibitor cocktail (Beyotime). For in vitro experiments, C2C12 cells were seeded at a density of 2×10^5 cells/well in six-well plates and differentiated for 5 days. After treatment with palmitate and *FYGL*, cells were lysed in lysis buffer. Muscle homogenates and whole cell lysates were centrifuged at 12,000 × *g* for 10 min at 4 °C to remove insoluble materials. The supernatants were collected, and the total protein concentration was determined using the BCA protein assay kit (Beyotime). Equal amounts (20−50 μg) of protein were subjected to 10% SDS-PAGE and transferred to PVDF membranes (Beyotime). The membranes were blocked with 5% BSA for 1 h, stained with primary antibodies at 4 °C overnight, and then with horseradish peroxidase-conjugated secondary antibodies (Beyotime). The immune complexes were tested using the BeyoECL Star kit (Beyotime), and the band density was quantified via Image J software. Anti-AKT (1:1000), anti-phospho-AKT (Ser473; 1:2000), anti-AMPK (1:1000), and anti-p-AMPK (Thr172; 1:1000) were supplied by Cell Signaling Technology (Danvers, MA, USA). Anti-SIRT1 (1:1000) and anti-atrogin1(1:1000) were purchased from Abcam (Cambridge, MA, USA). Anti-β-Actin (1:4000) was obtained from Yeasen Biotechnology Co., Ltd. (Shanghai, China).

5.13. Statistical Analysis. All experiments were performed in triplicate at a minimum. Statistical analyses were conducted using SPSS 19.0 (SPSS, Inc., Chicago, IL, USA) using one-way ANOVA and Tukey's post hoc test. All data are presented as mean ± SEM. Differences at $P < 0.05$ was considered statistically significant.

■ ASSOCIATED CONTENT

Supporting Information

The Supporting Information is available free of charge at https://pubs.acs.org/doi/10.1021/acsomega.3c03513.

^{1}H-NMR spectrum of *FYGL* in D_2O (S1); ^{13}C-NMR spectrum of *FYGL* in D_2O (S2); ^{1}H−^{13}C HSQC NMR spectra of anomeric groups in *FYGL* in D_2O (S3); ^{1}H−^{1}H COSY NMR spectra of anomeric groups in *FYGL* in D_2O (S4); ^{1}H−^{1}H TOCSY NMR spectra of anomeric groups in *FYGL* in D_2O (S5);^{1}H−^{13}C HMBC NMR spectra of anomeric groups in *FYGL* in D_2O (S6); effects of *FYGL* on FBG and body weight in T2D rats (S7); effects of *FYGL* on FBG and body weight in T2D mice (S8); ultraviolet spectrum of FITC, *FYGL*, and FITC-*FYGL* (S9); and top pathways regulated by *FYGL* in *db/db* mice according to KEGG enrichment (S10) (PDF)

■ AUTHOR INFORMATION

Corresponding Authors

Yanming He − *Yueyang Hospital of Integrated Traditional Chinese and Western Medicine, Shanghai University of Traditional Chinese Medicine, Shanghai 200437, China*; Email: heyanming176@163.com

Hongjie Yang − *Yueyang Hospital of Integrated Traditional Chinese and Western Medicine, Shanghai University of Traditional Chinese Medicine, Shanghai 200437, China*; Email: yanghongjie1964@aliyun.com

Ping Zhou − *State Key Laboratory of Molecular Engineering of Polymers, Department of Macromolecular Science, Fudan University, Shanghai 200433, China*; orcid.org/0000-0002-5954-7655; Email: pingzhou@fudan.edu.cn; Fax: +86-21-3124-4038

Authors

Jiaqi Li − *State Key Laboratory of Molecular Engineering of Polymers, Department of Macromolecular Science, Fudan University, Shanghai 200433, China*

Ying Zhang − *State Key Laboratory of Molecular Engineering of Polymers, Department of Macromolecular Science, Fudan University, Shanghai 200433, China*

Fanzhen Yu − *State Key Laboratory of Molecular Engineering of Polymers, Department of Macromolecular Science, Fudan University, Shanghai 200433, China*

Yanna Pan − *State Key Laboratory of Molecular Engineering of Polymers, Department of Macromolecular Science, Fudan University, Shanghai 200433, China*

Zeng Zhang − *Yueyang Hospital of Integrated Traditional Chinese and Western Medicine, Shanghai University of Traditional Chinese Medicine, Shanghai 200437, China*

Complete contact information is available at: https://pubs.acs.org/10.1021/acsomega.3c03513

Notes

The authors declare no competing financial interest.

■ ACKNOWLEDGMENTS

The authors thank the National Natural Science Foundation of China (nos. 21374022 and 81374032), the National Health Commission of the People's Republic of China (no. 2017ZX09301006), the Science and Technology Commission of Shanghai Municipality (no. 17401902700), the Clinical Research Plan of SHDC (no. SHDC12019124), and the Shanghai Collaborative Innovation Center of Industrial Transformation of Hospital TCM Preparation for financial support.

REFERENCES

(1) Kalyani, R. R.; Corriere, M.; Ferrucci, L. Age-related and disease-related muscle loss: the effect of diabetes, obesity, and other diseases. *Lancet Diabetes Endocrinol.* **2014**, *2*, 819−829.

(2) Song, J.; Liu, J.; Cui, C.; Hu, H.; Zang, N.; Yang, M.; Yang, J.; Zou, Y.; Li, J.; Wang, L.; et al. Mesenchymal stromal cells ameliorate diabetes-induced muscle atrophy through exosomes by enhancing AMPK/ULK1-mediated autophagy. *J. Cachexia Sarcopenia Muscle* **2023**, 915.

(3) Lipina, C.; Hundal, H. S. Lipid modulation of skeletal muscle mass and function. *J. Cachexia Sarcopenia Muscle* **2017**, *8*, 190−201.

(4) Cohen, S.; Nathan, J. A.; Goldberg, A. L. Muscle wasting in disease: molecular mechanisms and promising therapies. *Nat. Rev. Drug Discovery* **2015**, *14*, 58−74.

(5) Hong, Y.; Lee, J. H.; Jeong, K. W.; Choi, C. S.; Jun, H.-S. Amelioration of muscle wasting by glucagon-like peptide-1 receptor agonist in muscle atrophy. *J. Cachexia Sarcopenia Muscle* **2019**, *10*, 903−918.

(6) Mounier, R.; Theret, M.; Lantier, L.; Foretz, M.; Viollet, B. Expanding roles for AMPK in skeletal muscle plasticity. *Trends Endocrinol. Metab.* **2015**, *26*, 275−286.

(7) Lagouge, M.; Argmann, C.; Gerhart-Hines, Z.; Meziane, H.; Lerin, C.; Daussin, F.; Messadeq, N.; Milne, J.; Lambert, P.; Elliott, P.; et al. Resveratrol improves mitochondrial function and protects against metabolic disease by activating SIRT1 and PGC-1 alpha. *Cell* **2006**, *127*, 1109−1122.

(8) Nikawa, T.; Ulla, A.; Sakakibara, I. Polyphenols and Their Effects on Muscle Atrophy and Muscle Health. *Molecules* **2021**, *26*, 4887.

(9) Kahn, B. B.; Alquier, T.; Carling, D.; Hardie, D. G. AMP-activated protein kinase: Ancient energy gauge provides clues to modern understanding of metabolism. *Cell Metab.* **2005**, *1*, 15−25.

(10) Chen, K.-H.; Cheng, M.-L.; Jing, Y.-H.; Chiu, D. T.-Y.; Shiao, M.-S.; Chen, J.-K. Resveratrol ameliorates metabolic disorders and muscle wasting in streptozotocin-induced diabetic rats. *Am. J. Physiol.: Endocrinol. Metab.* **2011**, *301*, E853−E863.

(11) Kou, X.; Li, J.; Liu, X.; Yang, X.; Fan, J.; Chen, N. Ampelopsin attenuates the atrophy of skeletal muscle from D-gal-induced aging rats through activating AMPK/SIRT1/PGC-1 alpha signaling cascade. *Biomed. Pharmacother.* **2017**, *90*, 311−320.

(12) Shen, S.; Liao, Q.; Liu, J.; Pan, R.; Lee, S. M.-Y.; Lin, L. Myricanol rescues dexamethasone-induced muscle dysfunction via a sirtuin 1-dependent mechanism. *J. Cachexia Sarcopenia Muscle* **2019**, *10*, 429−444.

(13) Kan, Y.; Chen, T.; Wu, Y.; Wu, J.; Wu, J. Antioxidant activity of polysaccharide extracted from Ganoderma lucidum using response surface methodology. *Int. J. Biol. Macromol.* **2015**, *72*, 151−157.

(14) Huang, C.-Y.; Chen, J. Y.-F.; Wu, J.-E.; Pu, Y.-S.; Liu, G.-Y.; Pan, M.-H.; Huang, Y.-T.; Huang, A. M.; Hwang, C.-C.; Chung, S.-J.; et al. Ling-zhi polysaccharides potentiate cytotoxic effects of anticancer drugs against drug-resistant urothelial carcinoma cells. *J. Agric. Food Chem.* **2010**, *58*, 8798−8805.

(15) Cao, Y.-J.; Huang, Z.-R.; You, S.-Z.; Guo, W.-L.; Zhang, F.; Liu, B.; Lv, X.-C.; Lin, Z.-X.; Liu, P.-H. The Protective Effects of Ganoderic Acids from Ganoderma lucidum Fruiting Body on Alcoholic Liver Injury and Intestinal Microflora Disturbance in Mice with Excessive Alcohol Intake. *Foods* **2022**, *11*, 949.

(16) Teng, B.-S.; Wang, C.-D.; Yang, H.-J.; Wu, J.-S.; Zhang, D.; Zheng, M.; Fan, Z.-H.; Pan, D.; Zhou, P. A Protein Tyrosine Phosphatase 1B Activity Inhibitor from the Fruiting Bodies of Ganoderma lucidum (Fr.) Karst and Its Hypoglycemic Potency on Streptozotocin-Induced Type 2 Diabetic Mice. *J. Agric. Food Chem.* **2011**, *59*, 6492−6500.

(17) Pan, D.; Wang, L.; Chen, C.; Hu, B.; Zhou, P. Isolation and characterization of a hyperbranched proteoglycan from Ganoderma Lucidum for anti-diabetes. *Carbohydr. Polym.* **2015**, *117*, 106−114.

(18) Yu, F.; Wang, Y.; Teng, Y.; Yang, S.; He, Y.; Zhang, Z.; Yang, H.; Ding, C.-F.; Zhou, P. Interaction and Inhibition of a Ganoderma lucidum Proteoglycan on PTP1B Activity for Anti-diabetes. *ACS Omega* **2021**, *6*, 29804−29813.

(19) Yang, Z.; Wu, F.; He, Y.; Zhang, Q.; Zhang, Y.; Zhou, G.; Yang, H.; Zhou, P. A novel PTP1B inhibitor extracted from Ganoderma lucidum ameliorates insulin resistance by regulating IRS1-GLUT4 cascades in the insulin signaling pathway. *Food Funct.* **2018**, *9*, 397−406.

(20) Jung, T. W.; Hwang, H.-J.; Hong, H. C.; Yoo, H. J.; Baik, S. H.; Choi, K. M. BAIBA attenuates insulin resistance and inflammation induced by palmitate or a high fat diet via an AMPK-PPAR delta-dependent pathway in mice. *Diabetologia* **2015**, *58*, 2096−2105.

(21) Jung, T. W.; Lee, S. H.; Kim, H.-C.; Bang, J. S.; Abd El-Aty, A. M.; Hacimuftuoglu, A.; Shin, Y. K.; Jeong, J. H. METRNL attenuates lipid-induced inflammation and insulin resistance via AMPK or PPARdelta-dependent pathways in skeletal muscle of mice. *Exp. Mol. Med.* **2018**, *50*, 1−11.

(22) Bryner, R. W.; Woodworth-Hobbs, M. E.; Williamson, D. L.; Alway, S. E. Docosahexaenoic Acid protects muscle cells from palmitate-induced atrophy. *ISRN Obes.* **2012**, *2012*, 647348−647348.

(23) Woodworth-Hobbs, M. E.; Hudson, M. B.; Rahnert, J. A.; Zheng, B.; Franch, H. A.; Price, S. R. Docosahexaenoic acid prevents palmitate-induced activation of proteolytic systems in C2C12 myotubes. *J. Nutr. Biochem.* **2014**, *25*, 868−874.

(24) Yu, F.; Teng, Y.; Yang, S.; He, Y.; Zhang, Z.; Yang, H.; Ding, C.-F.; Zhou, P. The thermodynamic and kinetic mechanisms of a Ganoderma lucidum proteoglycan inhibiting hIAPP amyloidosis. *Biophys. Chem.* **2022**, *280*, No. 106702.

(25) Yu, F.; Teng, Y.; Li, J.; Yang, S.; Zhang, Z.; He, Y.; Yang, H.; Ding, C.-F.; Zhou, P. Effects of a Ganoderma lucidum Proteoglycan on Type 2 Diabetic Rats and the Recovery of Rat Pancreatic Islets. *ACS Omega* **2023**, *8*, 17304−17316.

(26) Thomas, M.; Langley, B.; Berry, C.; Sharma, M.; Kirk, S.; Bass, J.; Kambadur, R. Myostatin, a negative regulator of muscle growth, functions by inhibiting myoblast proliferation. *J. Biol. Chem.* **2000**, *275*, 40235−40243.

(27) Sartori, R.; Milan, G.; Patron, M.; Mammucari, C.; Blaauw, B.; Abraham, R.; Sandri, M. Smad2 and 3 transcription factors control muscle mass in adulthood. *Am. J. Physiol.: Cell Physiol.* **2009**, *296*, C1248−C1257.

(28) Han, H. Q.; Zhou, X.; Mitch, W. E.; Goldberg, A. L. Myostatin/activin pathway antagonism: Molecular basis and therapeutic potential. *Int. J. Biochem. Cell Biol.* **2013**, *45*, 2333−2347.

(29) Pan, Y.; Yuan, S.; Teng, Y.; Zhang, Z.; He, Y.; Zhang, Y.; Liang, H.; Wu, X.; Li, J.; Yang, H.; et al. Antioxidation of a proteoglycan from Ganoderma lucidum protects pancreatic beta-cells against oxidative stress-induced apoptosis in vitro and in vivo. *Int. J. Biol. Macromol.* **2022**, *200*, 470−486.

(30) Halevy, O.; Novitch, B. G.; Spicer, D. B.; Skapek, S. X.; Rhee, J.; Hannon, G. J.; Beach, D.; Lassar, A. B. Correlation of terminal cell-cycle arrest of skeletal-muscle with induction of p21 by MyoD. *Science* **1995**, *267*, 1018−1021.

(31) Xiao, F.; Wang, H.; Fu, X.; Li, Y.; Ma, K.; Sun, L.; Gao, X.; Wu, Z. Oncostatin M inhibits myoblast differentiation and regulates muscle regeneration. *Cell Res.* **2011**, *21*, 350−364.

(32) Schiaffino, S.; Mammucari, C. Regulation of skeletal muscle growth by the IGF1-Akt/PKB pathway: insights from genetic models. *Skeletal Muscle* **2011**, *1*, 4−4.

(33) Trendelenburg, A. U.; Meyer, A.; Rohner, D.; Boyle, J.; Hatakeyama, S.; Glass, D. J. Myostatin reduces Akt/TORC1/p70S6K signaling, inhibiting myoblast differentiation and myotube size. *Am. J. Physiol.: Cell Physiol.* **2009**, *296*, C1258−C1270.

(34) Kang, J. S.; Mulieri, P. J.; Miller, C.; Sassoon, D. A.; Krauss, R. S. CDO, a Robo-related cell surface protein that mediates myogenic differentiation. *J. Cell Biol.* **1998**, *143*, 403−413.

(35) Blumer, M.; Brown, T.; Freitas, M. B.; Destro, A. L.; Oliveira, J. A.; Morales, A. E.; Schell, T.; Greve, C.; Pippel, M.; Jebb, D.; et al. Gene losses in the common vampire bat illuminate molecular adaptations to blood feeding. *Sci. Adv.* **2022**, *8*, No. eabm6494.

(36) Mootha, V. K.; Lindgren, C. M.; Eriksson, K. F.; Subramanian, A.; Sihag, S.; Lehar, J.; Puigserver, P.; Carlsson, E.; Ridderstrale, M.; Laurila, E.; et al. PGC-1 alpha-responsive genes involved in oxidative

https://doi.org/10.1021/acsomega.3c03513
ACS Omega 2023, 8, 30359−30373

phosphorylation are coordinately downregulated in human diabetes. *Nat. Genet.* **2003**, *34*, 267−273.
(37) Reza, M. M.; Subramaniyam, N.; Sim, C. M.; Ge, X.; Sathiakumar, D.; McFarlane, C.; Sharma, M.; Kambadur, R. Irisin is a pro-myogenic factor that induces skeletal muscle hypertrophy and rescues denervation-induced atrophy. *Nat. Commun.* **2017**, *8*, 1104.
(38) Kong, D.; He, M.; Yang, L.; Zhou, R.; Yan, Y.-Q.; Liang, Y.; Teng, C.-B. MiR-17 and miR-19 cooperatively promote skeletal muscle cell differentiation. *Cell. Mol. Life Sci.* **2019**, *76*, 5041−5054.
(39) Samuel, V. T.; Shulman, G. I. Mechanisms for insulin resistance: common threads and missing links. *Cell* **2012**, *148*, 852−871.
(40) Sadeghi, A.; Ebrahimi, S. S. S.; Golestani, A.; Meshkani, R. Resveratrol Ameliorates Palmitate-Induced Inflammation in Skeletal Muscle Cells by Attenuating Oxidative Stress and JNK/NF-kappa B Pathway in a SIRT1-Independent Mechanism. *J. Cell. Biochem.* **2017**, *118*, 2654−2663.
(41) D'Souza, D. M.; Al-Sajee, D.; Hawke, T. J. Diabetic rnyopathy: impact of diabetes mellitus on skeletal muscle progenitor cells. *Front. Physiol.* **2013**, *4*, 379.
(42) Teng, Y.; Liang, H.; Zhang, Z.; He, Y.; Pan, Y.; Yuan, S.; Wu, X.; Zhao, Q.; Yang, H.; Zhou, P. Biodistribution and immunomodulatory activities of a proteoglycan isolated from Ganoderma lucidum. *J. Funct. Foods* **2020**, *74*, No. 104193.
(43) Li, Q.; Yang, H.; Song, S.; Liu, J.; Wang, Z.; Wang, J. Bioactive Components in Whole Grains for the Regulation of Skeletal Muscle Function. *Foods* **2022**, *11*, 2752.
(44) Mukai, R.; Nakao, R.; Yamamoto, H.; Nikawa, T.; Takeda, E.; Terao, J. Quercetin Prevents Unloading-Derived Disused Muscle Atrophy by Attenuating the Induction of Ubiquitin Ligases in Tail-Suspension Mice. *J. Nat. Prod.* **2010**, *73*, 1708−1710.
(45) Tsubouchi, H.; Yanagi, S.; Miura, A.; Matsumoto, N.; Kangawa, K.; Nakazato, M. Ghrelin relieves cancer cachexia associated with the development of lung adenocarcinoma in mice. *Eur. J. Pharmacol.* **2014**, *743*, 1−10.
(46) Gupta, P.; Bala, M.; Gupta, S.; Dua, A.; Dabur, R.; Injeti, E.; Mittal, A. Efficacy and risk profile of anti-diabetic therapies: Conventional vs traditional drugs-A mechanistic revisit to understand their mode of action. *Pharmacol. Res.* **2016**, *113*, 636−674.
(47) Andreozzi, F.; Raciti, G. A.; Nigro, C.; Mannino, G. C.; Procopio, T.; Davalli, A. M.; Beguinot, F.; Sesti, G.; Miele, C.; Folli, F. The GLP-1 receptor agonists exenatide and liraglutide activate Glucose transport by an AMPK-dependent mechanism. *J. Transl. Med.* **2016**, *14*, 229.
(48) Jesinkey, S. R.; Korrapati, M. C.; Rasbach, K. A.; Beeson, C. C.; Schnellmann, R. G. Atomoxetine Prevents Dexamethasone-Induced Skeletal Muscle Atrophy in Mice. *J. Pharmacol. Exp. Ther.* **2014**, *351*, 663−673.
(49) Ou, H.-C.; Chu, P.-M.; Huang, Y.-T.; Cheng, H.-C.; Chou, W.-C.; Yang, H.-L.; Chen, H.-I.; Tsai, K.-L. Low-level laser prevents doxorubicin-induced skeletal muscle atrophy by modulating AMPK/SIRT1/PCG-1 alpha-mediated mitochondrial function, apoptosis and up-regulation of pro-inflammatory responses. *Cell Biosci.* **2021**, *11*, 200.
(50) Zhang, B. B.; Zhou, G.; Li, C. AMPK: an emerging drug target for diabetes and the metabolic syndrome. *Cell Metab.* **2009**, *9*, 407−416.
(51) Landgraf, R. R.; Goswami, D.; Rajamohan, F.; Harris, M. S.; Calabrese, M. F.; Hoth, L. R.; Magyar, R.; Pascal, B. D.; Chalmers, M. J.; Busby, S. A.; et al. Activation of AMP-activated protein kinase revealed by hydrogen/deuterium exchange mass spectrometry. *Structure* **2013**, *21*, 1942−1953.
(52) Goeransson, O.; McBride, A.; Hawley, S. A.; Ross, F. A.; Shpiro, N.; Foretz, M.; Viollet, B.; Hardie, D. G.; Sakamoto, K. Mechanism of action of A-769662, a valuable tool for activation of AMP-activated protein kinase. *J. Biol. Chem.* **2007**, *282*, 32549−32560.
(53) Cool, B.; Zinker, B.; Chiou, W.; Kifle, L.; Cao, N.; Perham, M.; Dickinson, R.; Adler, A.; Gagne, G.; Iyengar, R.; et al. Identification and characterization of a small molecule AMPK activator that treats key components of type 2 diabetes and the metabolic syndrome. *Cell Metab.* **2006**, *3*, 403−416.
(54) Calabrese, M. F.; Rajamohan, F.; Harris, M. S.; Caspers, N. L.; Magyar, R.; Withka, J. M.; Wang, H.; Borzilleri, K. A.; Sahasrabudhe, P. V.; Hoth, L. R.; et al. Structural basis for AMPK activation: natural and synthetic ligands regulate kinase activity from opposite poles by different molecular mechanisms. *Structure* **2014**, *22*, 1161−1172.
(55) Nishida, Y.; Nawaz, A.; Kado, T.; Takikawa, A.; Igarashi, Y.; Onogi, Y.; Wada, T.; Sasaoka, T.; Yamamoto, S.; Sasahara, M.; et al. Astaxanthin stimulates mitochondrial biogenesis in insulin resistant muscle via activation of AMPK pathway. *J. Cachexia Sarcopenia Muscle* **2020**, *11*, 241−258.
(56) Ahn, J.; Lee, H.; Kim, S.; Park, J.; Ha, T. The anti-obesity effect of quercetin is mediated by the AMPK and MAPK signaling pathways. *Biochem. Biophys. Res. Commun.* **2008**, *373*, 545−549.
(57) Hawley, S. A.; Ford, R. J.; Smith, B. K.; Gowans, G. J.; Mancini, S. J.; Pitt, R. D.; Day, E. A.; Salt, I. P.; Steinberg, G. R.; Hardie, D. G. The Na+/Glucose Cotransporter Inhibitor Canagliflozin Activates AMPK by Inhibiting Mitochondrial Function and Increasing Cellular AMP Levels. *Diabetes* **2016**, *65*, 2784−2794.
(58) Liu, J.; Sun, D.; Zhu, J.; Liu, C.; Liu, W. Carbohydrate-binding modules targeting branched polysaccharides: overcoming side-chain recalcitrance in a non-catalytic approach. *Bioresour. Bioprocess.* **2021**, *8*, 28.
(59) Latres, E.; Amini, A. R.; Amini, A. A.; Griffiths, J.; Martin, F. J.; Wei, Y.; Lin, H. C.; Yancopoulos, G. D.; Glass, D. J. Insulin-like growth factor-1 (IGF-1) inversely regulates atrophy-induced genes via the phosphatidylinositol 3-kinase/Akt/mammalian target of rapamycin (PI3K/Akt/mTOR) pathway. *J. Biol. Chem.* **2005**, *280*, 2737−2744.
(60) You, J.-S.; Kim, K.; Steinert, N. D.; Chen, J.; Hornberger, T. A. mTORC1 mediates fiber type-specific regulation of protein synthesis and muscle size during denervation. *Cell Death Discovery* **2021**, *7*, 74.
(61) Teng, B. S.; Wang, C. D.; Zhang, D.; Wu, J. S.; Pan, D.; Pan, L. F.; Yang, H. J.; Zhou, P. Hypoglycemic effect and mechanism of a proteoglycan from Ganoderma Lucidum on streptozotocin-induced type 2 diabetic rats. *Eur. Rev. Med. Pharmacol. Sci.* **2012**, *16*, 166−175.
(62) Ohashi, K.; Ishikawa, K.; Maruyama, K. FITC-Labeled I-protein specifically binds to A-bands and or Z-lines of glycerinated myofibrils of chicken breast muscle. *J. Biochem.* **1988**, *103*, 367−369.

https://doi.org/10.1021/acsomega.3c03513
ACS Omega 2023, 8, 30359−30373